Radio Science, Volume 35, Number 3, Pages 885–904, May–June 2000

The application of GPS observations to equatorial aeronomy

Michael Mendillo, Bosheng Lin, and Jules Aarons
Center for Space Physics, Boston University, Boston, Massachusetts

Abstract. Routine observations of the ionospherically imposed propagation effects upon GPS satellite signals are available online from the International GPS Service for Geodynamics. With over 200 ground-based stations now reporting data, ionospheric studies ranging from the analysis of single-site observations to the full global network have demonstrated the geophysical science yield possible from this remarkable resource. In this paper we expand on the use of GPS data for comprehensive "regional studies" at low latitudes. Using the GPS observing sites in South America, we show how routine observations are processed to form reliable total electron content(TEC) values capable of describing the latitudinal, longitudinal, local time, and storm time behavior over the full span of the continent. To study the dominant F region structure at low latitudes, the Appleton anomaly, two indices are developed to assess its strength (I_s) and asymmetry (I_a). TEC data at 30 s intervals are used to form phase fluctuation indices that capture plasma irregularity patterns at 15-min (f_p) and hourly (F_P) time resolution. Tests of F_P at Atlantic and Pacific sector locations show them to reproduce accurately all known occurrence patterns for equatorial spread F (ESF). The use of the three indices (I_s, I_a, and F_P) to formulate predictive capabilities for ESF on the basis of the enhancement or suppression of growth rate indicators was not particularly successful.

1. Introduction

Global Positioning System (GPS) satellites offer a remarkable new way to study ionospheric structure and associated perturbations. A series of pilot studies have been conducted to demonstrate the techniques employed [*Lanyi and Roth*, 1988; *Wilson et al.*, 1995; *Mannucci et al.*, 1998] and the comparative accuracies possible [*Imel*, 1994; *Ciraolo and Spalla*, 1997; *Ho et al.*, 1997]. While initial attention to the ionospheric science yield from GPS measurements dealt with single-site measurements [*Coker et al.*, 1995], it was quickly appreciated that the scope of using GPS data could expand to several sites at high latitudes [*Aarons*, 1997] or low latitudes [*Aarons et al.*, 1996, 1997]. In a powerful demonstration of global network techniques, several Jet Propulsion Laboratory (JPL) studies showed how ionospheric storms could be monitored, potentially in near real time, to describe global effects [*Ho et al.*, 1996, 1998a, b; *Pi et al.*, 1997] and their comparison with TIEGCM models [*Lu et al.*, 1998].

GPS data are available from the International GPS Service (IGS) for Geodynamics. In a short period of time the IGS has developed a worldwide network of GPS satellite tracking stations, data centers, and analysis systems that put high-quality GPS data and data products on line, in near real time, to meet the needs of a wide range of geophysical science and engineering applications. Currently, there are ~200 stations that collect and archive daily observations in standard receiver independent exchange (RINEX) format.

In this paper, we describe several GPS analysis techniques developed to study outstanding science issues in equatorial aeronomy. In focusing on a specific world region, the low-latitude zone, we hope to

Paper number 1999RS002208.
0048-6604/00/1999RS002208$11.00

show how simple F region integrated quantities can be used to examine regional upper atmosphere processes, that is, effects that potentially elude single-site measurements and global investigations. The global ionosonde network was the first to document equatorial F region morphology, discovering the Appleton anomaly and, of course, the HF sounding disruptions that came to be known as equatorial spread F (ESF). The impact of GPS studies could be as productive scientifically as those from the ionosonde network, particularly in the areas of F region storms and ESF patterns.

We begin with a brief discussion of methods to derive the equivalent vertical total electron content (TEC) from GPS signals, defined as

$$\mathrm{TEC} = \int N_e(h)dh, \tag{1}$$

and then the rate of change of TEC using 30 s TEC data sets to portray plasma irregularity patterns. While these two parameters, measures of integrated ionospheric structure and medium-scale irregularities, are limited data sets in comparison to those from multi-instrumented satellites capable of global in situ observations or to the multi parameter results from incoherent scatter radars at 6-8 sites worldwide, the ultimate benefit of GPS observations is in the sheer volume of data afforded by simultaneous observations at so many sites. Moreover, the continuity of observations allows for the complete study of storm effects, from quiet to disturbed to recovery phases.

Figure 1 shows the current network of IGS stations at low latitudes capable of supporting such "regional studies" of the ionosphere. Each station is equipped with a GPS receiver that can track between 4 and 12 satellites at a given time over an essentially all-sky geometry. With the number of such stations continuing to grow, coverage of the equatorial zone on a truly global scale will soon be possible. Here we attempt to show how such data can be used to address both applications needs in communications and science questions in the equatorial zone. To do this, we concentrate primarily on the South American equatorial sector as the beginning of global studies of equatorial irregularity development.

2. Data Sources and Analysis Methods

2.1. Reduction of GPS Signals to Geophysical Parameters

Several authors have described the detailed methods and associated uncertainties in transforming raw GPS signals to meaningful ionospheric parameters. GPS provides phase measurement and pseudo-range measurement. Briefly, each GPS satellite transmits two carrier frequencies ($L1$=1.57542 GHz, and $L2$= 1.22760 GHz) that are affected by the thermal plasma along its ray path to a ground receiver. The time delays suffered due to the total electron content along the slant path (STEC) are called pseudo-range

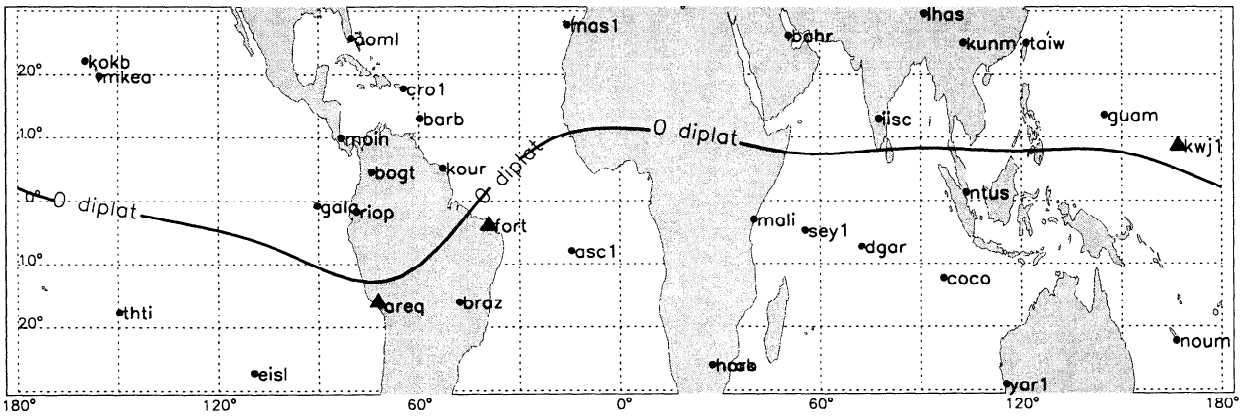

Figure 1. Geographic locations of GPS stations at low latitudes in the IGS network. Arequipa, Fortaleza, and Kwajalein, three stations marked by triangles, are used to portray effects in equatorial plasma irregularities at longitudes where the geomagnetic field declinations differ significantly.

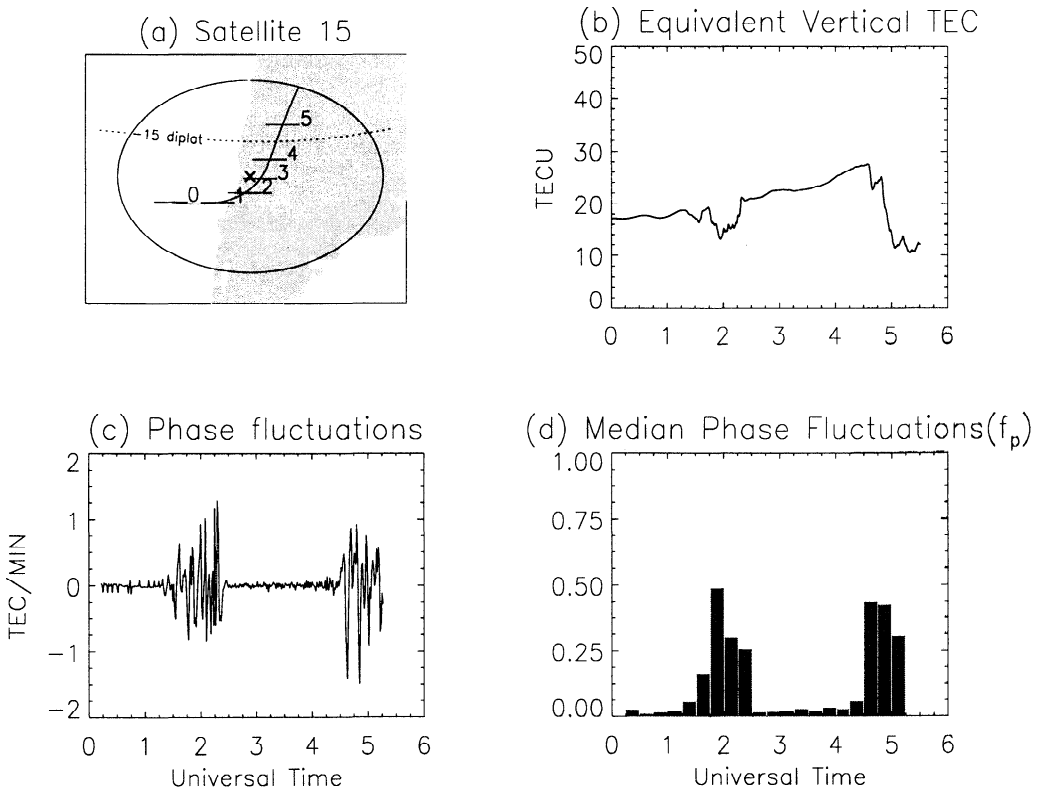

Figure 2. (a) The pass of GPS satellite 15, as recorded by the IGS station in Santiago, Chile, on October 23, 1996. The circle is at 400 km height and 15° elevation angle, corresponding to a field of view ~1000 km radius. (b) The equivalent vertical TEC, in units of 10^{16}el/m^2, is plotted as a function of universal time. (c) The corresponding total electron content (TEC) rate of change obtained from satellite 15. (d) An index for median phase fluctuations during 15 min periods shown in Figure 2c (see text). The large depletions shown in Figure 2b contain smaller-scale irregularities that cause the phase fluctuations shown in Figure 2c, and their parameterization in Figure 2d can be used for studies of such equatorial spread F (ESF) events.

$(P1, P2)$ errors because they would give a false incremental distance to the satellite (i.e., if one assumed that $L1$ and $L2$ traveled precisely at the in vacuo speed of light). This "ionospheric correction" must be performed before accurate geolocation calculations can be made. This potential error for the navigator is valued data for the space physicist. Since the GPS satellite's orbit is at an altitude of 20,200 km, the pseudo-range error represents the sum of ionospheric and plasmaspheric electron contents along the slant path, a point considered in more detail below.

The range error (or STEC) can be determined from these dual-frequency pseudo-range $(P1, P2)$ or carrier phase $(L1, L2)$ measurements. The pseudo-range or group delay measurement represents an absolute measure of the ionospheric range error in meters. The differential carrier phase measurement provides a much more precise measurement of the ionospheric error but only on a relative scale. In processing the data the accurate phase measurement is fit to the noisy pseudo-range measurement to obtain an absolute measurement of STEC. This fit is determined with data collected during the middle of the satellite pass to avoid the noisy data at low elevation angles and multipath interference. The vertical TEC can be calculated using

$$\text{TEC} = (\text{STEC} - C)/S \tag{2}$$

$$S = \sqrt{1 - [R/(R+h)]^2 \cos^2 el} \quad (3)$$

where R is the radius of the Earth and el is the elevation angle. On the basis of past modeling, the altitude h is set to 400 km, representing the height along the slanted ray path where the conversion to equivalent vertical TEC is made; the subionospheric coordinates of this point determine the derived value's latitude and longitude location. The offset (bias) C contains the dispersive delays in the transmitting and receiving equipment. While the satellite bias is relatively fixed for each satellite upon launch, the receiver biases can change for any number of operational reasons, and thus obtaining absolute TEC is a processs fraught with uncertainties.

The reduction method we employ for GPS data is illustrated in Figure 2. Figure 2a gives an example for the satellite 15 pass as observed from Santiago, Chile. The circle is at a 400 km height and 15° elevation angle, giving a usable field of view of ~1000 km in radius. The equivalent vertical TEC, in units of 10^{16} el/m^2, is plotted in Figure 2b as a function of universal time (UT). This represents a portion of the diurnal TEC pattern sampled by satellite 15 at these times. Two TEC depletions are clearly shown near 0200 and 0500 UT. These are signatures of F region plasma "bubbles" as the GPS ray path encounters depleted flux tubes of equatorial spread F (ESF) events in the postsunset and midnight periods. Within these large-scale depletions are smaller scale irregularities. A GPS ray path samples these as a rate of change of TEC per minute, that is, ΔTEC/Δt, measured by virtue of the "phase fluctuations" they cause. To isolate phase fluctuation data, we use a high-pass filter to eliminate the low frequency temporal component of TEC data and then examine the remaining variability. Figure 2c shows such an example of TEC rate of change obtained from satellite 15. While associated here with ESF, phase fluctuations occur at all latitudes in response to ionospheric irregularities. As discussed in section 2.4, we follow the convention of calling these phase fluctuations to emphasize their observational origin, just as amplitude scintillation is used in the ionospheric literature. Both are caused by plasma irregularities, the former large scale (ΔTEC) and the latter small scale (ΔNe).

2.2. Uncertainties

In addition to technological uncertainties (the transmitter and receiver biases noted above), there are geophysical factors that affect the portrayal of absolute, equivalent vertical TEC values. These fall into two general categories: (1) the use of a simple slab model at a fixed height (400 km) to convert slant TEC to vertical TEC ignores the presence of latitude and longitude gradients, (2) the removal of the plasmaspheric TEC component within the STEC in the hope of portraying "true ionospheric" TEC measurements.

These concerns are real and occasionally substantial. They are as old as the use of the TEC technique, starting with low-orbit satellite radio beacon measurements in the 1960s and continuing to the geostationary satellite beacon data of the 1970-1990s (see *Davies* [1980] for a review). They transcend differential Doppler, Faraday rotation, and group delay measurements. Model studies of various gradients and procedures to handle plasmaspheric contents have been conducted in many ways [*Titheridge*, 1972; *Mendillo and Klobuchar*, 1974]. On the basis of these long-standing results we adjust the minimum value of TEC at each site during a period of extended, continuous data (usually one month) to be in the range of 2-4 TEC units 10^{16} el/m^2. This, in principle, allows for the actual minimal TEC (usually in the pre-dawn period); it does not include the additional 2-3 TEC units for the overlying plasmasphere [*Almeida*, 1974; *Kersley and Klobuchar*, 1978] during the solar minimum periods of concern in this study. When done by experienced practioners of TEC data, the resultant possible errors in absolute values are probably comparable to, or better than, the best available model results for the combined ionosphere-plasma-sphere system [*Anderson et al.*, 1998]. Thus, for continuous data sets this uncertainty in absolute TEC of a few TEC units is clearly the best one can do using simple, readily available means. Relative changes within a day, or in comparisons between days spanning a period when no biases were changed, are obviously much more accurate.

For the GPS TEC era to be successful, limitations to the data sets obtained must be understood. To place this within the context of previous methods of TEC investigations, one should realize that a single GPS satellite pass combines the worst characteristics of satellite beacons in low Earth orbit and geostationary orbit; the former has poor time coverage at the same place, while the latter offers no spatial information beyond the fixed penetration point where excellent time coverage is obtained. The issue of spatial

gradients being an additional negative aspect of the technique has been a particular agitation to modelers at high latitudes (R. Schunk, private communication, 1999) and in the equatorial zone (D. Anderson, private communication, 1999). It is certainly true that configurations of satellite-station spatial $Ne(h)$ gradient can be found to confound the conversion to vertical TEC values, just as spatial grid limitations in computer codes limit the portrayal of actual gradients and filamentary structures. GPS results have to be treated with caution in such cases, recalling that it purports to be no more than an integrated measurement, as with all past TEC studies. Yet dramatic changes in TEC are observed very frequently, and these relate one-to-one to dramatic spatial and temporal effects observed by other techniques (for example, with in situ data, as shown by *Mendillo et al.* [1974]). Thus the value of the GPS technique is not that it pushes the envelope of new geophysical observations, but rather that it provides so many satellites with widely separated penetration points that TEC can be monitored simultaneously at so many places. The potential science yield (within the inevitable uncertainty of ± 2-4 TEC units) is still a major asset for ionospheric research, one comparable to state-of-the-art techniques of most other methods, whether observational or modeling.

2.3. Sample Results: TEC

To demonstrate the use of GPS-derived TEC data for studies of equatorial aeronomy, the regional map in Figure 3 shows a network of stations in South America. The West Coast sites of Bogota, Arequipa, and Santiago offer a particularly appropriate chain to examine the latitudinal pattern that so dominates F region morphology at low latitudes: the equatorial ionization anomaly (EIA). At each site, all of the GPS determinations of TEC can be organized into a "data cube" of TEC, latitude, and time. For this chain the "common meridian" is taken to be at 75° W, and so the time relationship used is UT = LT + 5 hours. For such a case, subtle longitude effects to the east and west of the station are not taken into account, but rather all latitudes observed are assigned to a site's longitude. The individual station results are then merged in latitude to give the diurnal morphology over the full low-latitude zone. The monthly mean TEC pattern for the month of October 1996 is given in Figure 4. The well-known EIA (or Appleton anomaly) is obtained during the afternoon hours,

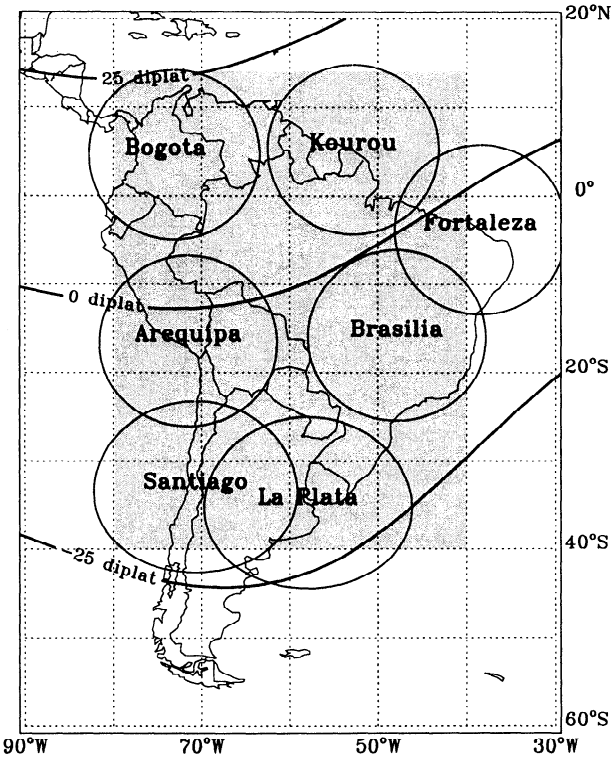

Figure 3. Network of GPS observing sites in South America. The circles at each site give the field of view for a 400 km intersection height at an elevation angle at 15°. Data points below 15° elevation angle are not used in any of these studies in order to avoid high noise and spatial gradient problems.

extending past midnight until it disappears in the predawn hours. The anomaly peaks are not symmetrical, suggesting that a northward wind is the dominant thermospheric meridional flow. In using the simple latitude-longitude-time bin approach we feel that spatial gradients are better preserved than if numerical curve fitting methods are employed. The latter are useful for more sparse data sets, as occurs for widely spaced oceanic sites.

To show the great variability found in the low-latitude ionosphere, Figure 5 gives the daily TEC latitude slices at 0030 UT (corresponding to 1930 LT). This is the time of the prereversal enhancement that affects so dramatically the distribution of low latitude plasma via the so-called fountain effect [*Anderson*, 1973, 1981; *Kelley*, 1989]. It should be emphasized that all GPS satellite and station biases

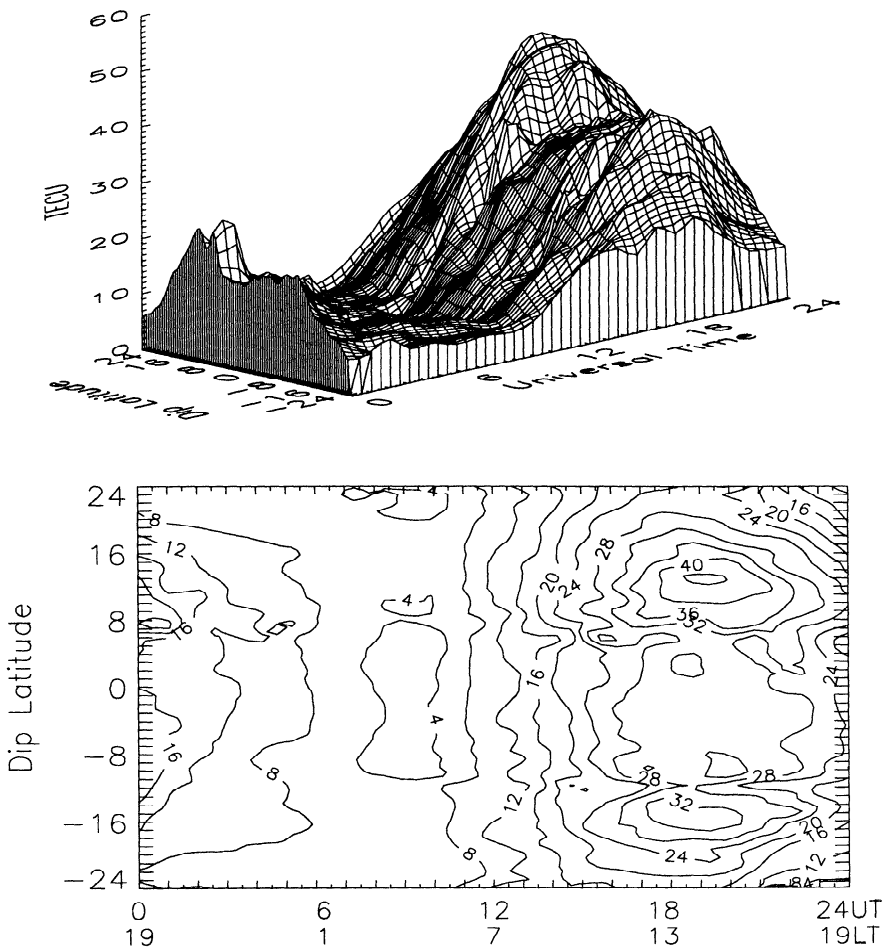

Figure 4. Three station monthly mean TEC plots derived from all GPS measurements in October 1996 from Bogota, Arequipa, and Santiago.

were kept constant for this month as part of our analysis protocol. The variability is thus a bonafide portrayal of the influence of variable electrodynamical drifts, thermospheric winds, and composition during this equinox month of absolute solar minimum ($\overline{F10.7} = 68.7, \overline{A}_p = 13$, a month of no reported solar flares). In section 3, we will show how day-to-day TEC patterns derived from GPS data can be used to search for ways such dynamics can affect the onset and evolution of equatorial spread F.

Figures 4 and 5 showed two ways to portray TEC, Figure 4 on a climatology basis and Figure 5 on a day-to-day basis. We have also investigated ways to use GPS data on a subdaily basis for specification of regional TEC patterns. Several approaches were tried to explore the trade-offs between temporal resolution and spatial coverage. We found that sufficient GPS passes occurred at each site in a 2 hour period to support portrayal of a spatial pattern across its field of view. Merging these patterns into a regional map of TEC over South America at 2 hour intervals is demonstrated in Plate 1. Four 2 hour periods are selected to illustrate the evolutionary pattern of the Appleton anomaly. In Plate 1a, as in other parts of the plate, the average local time at the center of the continental grid is appropriate for 60° W longitude, that is, LT = UT - 4 hours, or 0500 LT for the 0900 UT mean time. To the west in Plate 1a, the LT is 1 hour earlier and at the east end, 1 hour later. Thus, in the west (at 0400 LT) the Appleton anomaly is not present, and the emerging dayside ionosphere begins in the east (at 0600 LT). In Plate 1b the anomaly

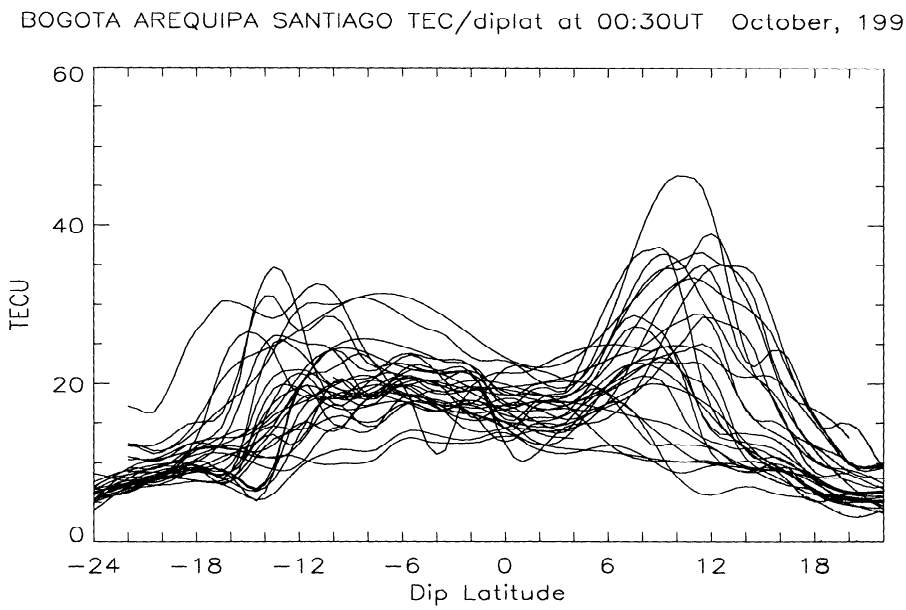

Figure 5. TEC latitude pattern obtained from merging three GPS stations (Bogata, Arequipa, and Santiago) in South America at 0030 UT(1930 LT) for each day in October 1996.

still has not yet developed 2 hours later in the west, but the fountain effect process is clearly underway at local noon in the east. In Plate 1c afternoon conditions occur across all of South America, and the Appleton anomaly is well formed at latitudes north and south of the geomagnetic equator. Finally, in Plate 1d the postsunset anomaly is particularly strong at 2100 LT, with the peak in the northern crest on this day being one of the strongest of the month. Such short-term specifications of TEC over an extensive region (in this case during an ionospheric storm) offer opportunities for data assimilation methods to be tried in regional and/or global simulation models. For example, the exceptionally strong anomaly at 2100 LT is the strongest case of the month, corresponding to the peak crests in both hemispheres shown in Figure 5. As a real-time data input, this would require that enhanced vertical drifts (eastward electric fields) be used to create a stronger anomaly. Yet the anomaly kept its basic asymmetry, suggesting that a storm time surge in transequatorial winds would not be needed in a model to keep simulation results consistent with actual developments in the region.

2.4. Sample Results: Phase Fluctuation Indices

As shown in Figure 2, the 30 s GPS data can be used to obtain TEC rate of change characteristics along a ray path. As in our earlier studies of irregularities at auroral [*Aarons*, 1997] and equatorial latitudes [*Aarons et al.*, 1996, 1997], we prefer to call these phase fluctuations. We do, however, retain the use of TEC units/min (rather than radians/s) in order to show how large the rate of change of TEC can be in comparison to the ambient TEC levels. The phase fluctuation designation is more readily comparable to the amplitude scintillation patterns long studied at low latitudes; the phrase "TEC fluctuations" is more general and might be confused with traveling ionospheric disturbances and storm effects.

It is important to note that each measurement technique biases the study relative to size of irregularities. In the case of phase fluctuations, one measures the rate of change of TEC over relatively large dimensions. At high elevation angles the satellite velocity encompasses a distance of ~6 km in the 60 s measurements we use. Thus only TEC irregularities

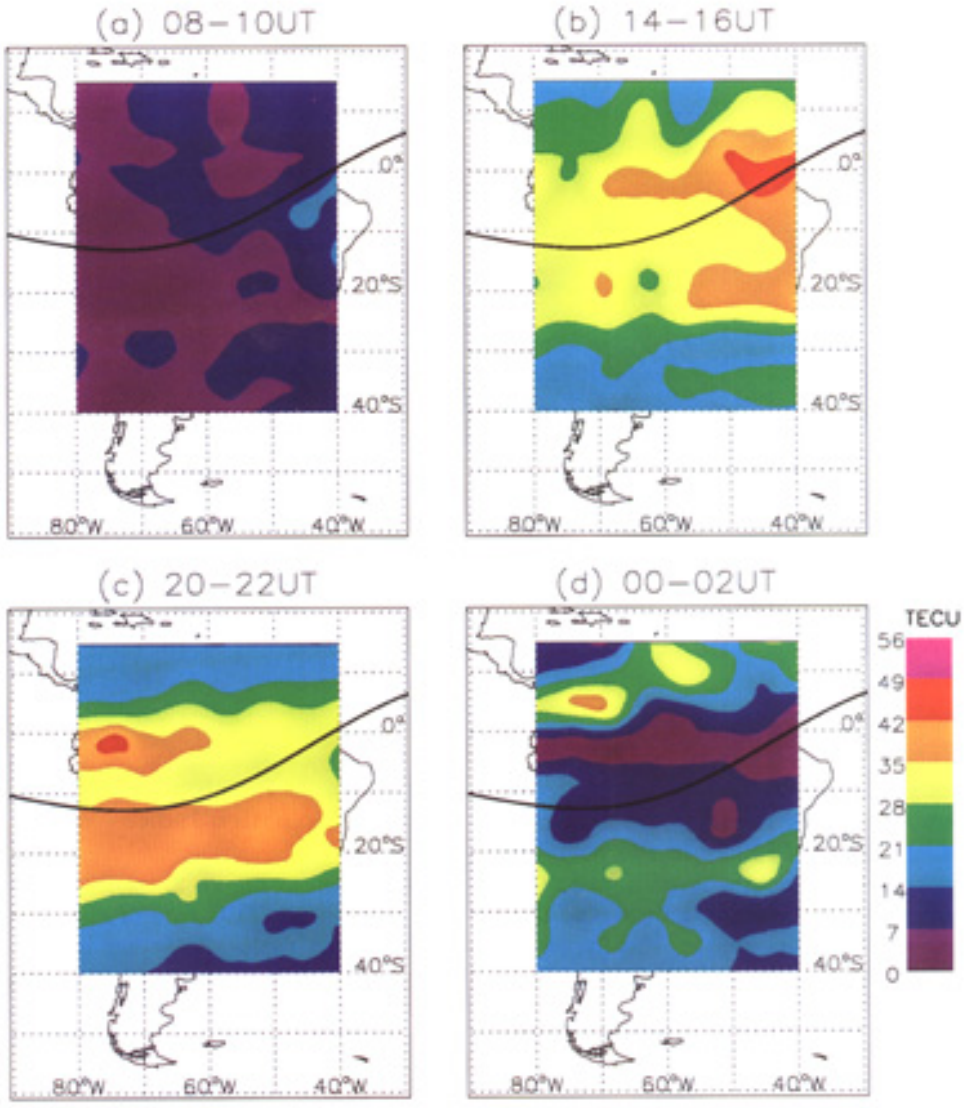

Plate 1. TEC "snapshots" derived from GPS observations over 2 hour intervals at seven stations in South America on October 23 1996. The UT time intervals and mean local times sampled are: (a) 0800-1000 UT (0500 LT), (b) 1400-1600 UT (1100 LT), (c) 2000-2200 UT (1700 LT), (d) 0000-0200 UT (2100 LT).

of this order are measured, rather than the spectra of phase fluctuations. In the case of GPS amplitude scintillations at the 1.6 GHz signal, the scale size of this scattering phenomenon is 350 m. Past amplitude scintillation data taken at meter wavelengths had an intermediate scale between these values. In addition to each type of measurement containing information of a particular scale size of plasma irregularity, amplitude scintillation is a scattering phenomenon [*Yeh and Liu*, 1982], and it may be confined to a narrow range of altitudes, while the TEC changes encompass, potentially, the entire path in the F region.

For the ESF studies of interest here, there is general agreement that the Rayleigh-Taylor instability produces an enormous range of scale sizes of plasma

irregularities. During the premidnight hours, 50 MHz radar backscatter caused by 3-m-scale irregularities coexist with the kilometer-scale irregularities that cause VHF amplitude scintillations [*Basu et al.*, 1978]. Similarly, the even larger scale (approximately several kilometers) irregularities studied in this paper coexist with the 400-m-scale irregularities that cause amplitude scintillation of the GPS signals. *Beach* and *Kintner* [1999] have recently presented an excellent description of GPS scale length effects.

Wanninger [1993] was apparently the first to suggest that 30 s RINEX data could be used to characterize "phase scintillations" as a diagnostic of ionospheric irregularities. He introduced an index for the rate of change of TEC (I_{ROT}) computed over a 15 min period by

$$\mathrm{I_{ROT}} = 10\mathrm{RMS}(\overline{\frac{\Delta \mathrm{TEC}}{\mathrm{min}}}) \tag{4}$$

Pi et al. [1997], concerned that smaller-scale fluctuations were not being identified, suggested that a rate of TEC index (ROTI) could be based on the standard deviation of ΔTEC/min over a 5 min interval, that is,

$$\mathrm{ROTI} = \sqrt{< \mathrm{ROT}^2 > - < \mathrm{ROT} >^2}. \tag{5}$$

The use of ROTI for global maps of irregularity occurrence and evolutions was demonstrated by *Pi et al.* [1997] for the ionospheric storm event of January 10, 1997.

For applications at low latitudes, where both climatological and event study issues are to be addressed, we see the need for indices that have the short time resolution required to study individual GPS satellite pass effects, as well as the broad patterns of occurrence at individual sites. Moreover, indices need to reject ever-present noise spikes if automated use of remote site observations are to be reliable for geophysical studies. Thus, to characterize phase fluctuations, we define the following two indices:

Index f_p, with 15 min time and space resolution, is the median value of the 60 s phase fluctuation data from one satellite over a 15 min period. Index f_p is always ≥ 0 and relates to a specific satellite pass at a specific site,

$$f_p(n, hr, i) = \mathrm{Median}\left|\frac{\Delta \mathrm{TEC}}{\mathrm{min}}\right|, \tag{6}$$

where n is the satellite number; hr is the hour(0000-2400 UT); i is the 15 min time section within an hour, and $i = 1, \cdots, 4$.

We find that the use of a median value effectively eliminates the noise spikes that might influence the earlier I_{ROT} and ROTI attempts. An example of the 15 min median phase fluctuation values (f_p) appears in Figure 2d.

F_P is an index with hourly resolution per site. F_P is the mean value of f_p from all the satellites observed at a site within 1 hour. F_P is intended to portray the general level of irregularities present in the vicinity of a given site.

$$F_P(hr) = \frac{\sum_n^{nsat}[\sum_i^k f_p(n, hr, i)/k]}{nsat(hr)} 1000; \tag{7}$$

where $nsat$ is the total number of satellites observed within an hour and k is the number of f_p values available within each hour ($k = 0, \cdots, 4$).

The multiplicative constant (1000) is used to make F_P an integer index. An F_P value ≤ 50 represents background levels of irregularities; $50 \leq F_P \leq 200$ signifies irregularities present, and when $F_P > 200$, it represents the occurrence of very strong irregularity levels.

Figure 6a shows the phase fluctuations from all GPS satellite signals for October 23, 1996, at Santiago, Chile. Two episodes we associated with ESF in Figure 2 (using satellite 15 only) are seen here to be part of the total sampling of ESF throughout the region, from 0100-0800 UT. Figure 6b shows the F_P index obtained from Figure 6a. The F_P index clearly captures the phase fluctuation patterns and is not contaminated by the noise spikes near 0130, 0800 and 1500 UT. In the following sections we use F_P to show its portrayal of ESF behavior in several ways.

3. Applications to Specific Equatorial Aeronomy Topics

The techniques described above apply to any site or region where GPS data are obtained. Here we address three specific issues in equatorial aeronomy where progress has been limited, in part, by lack of data in the region: occurrence patterns of ESF, predictions of ESF occurrence using precursor signatures, and behavior of the F region during ionospheric storms.

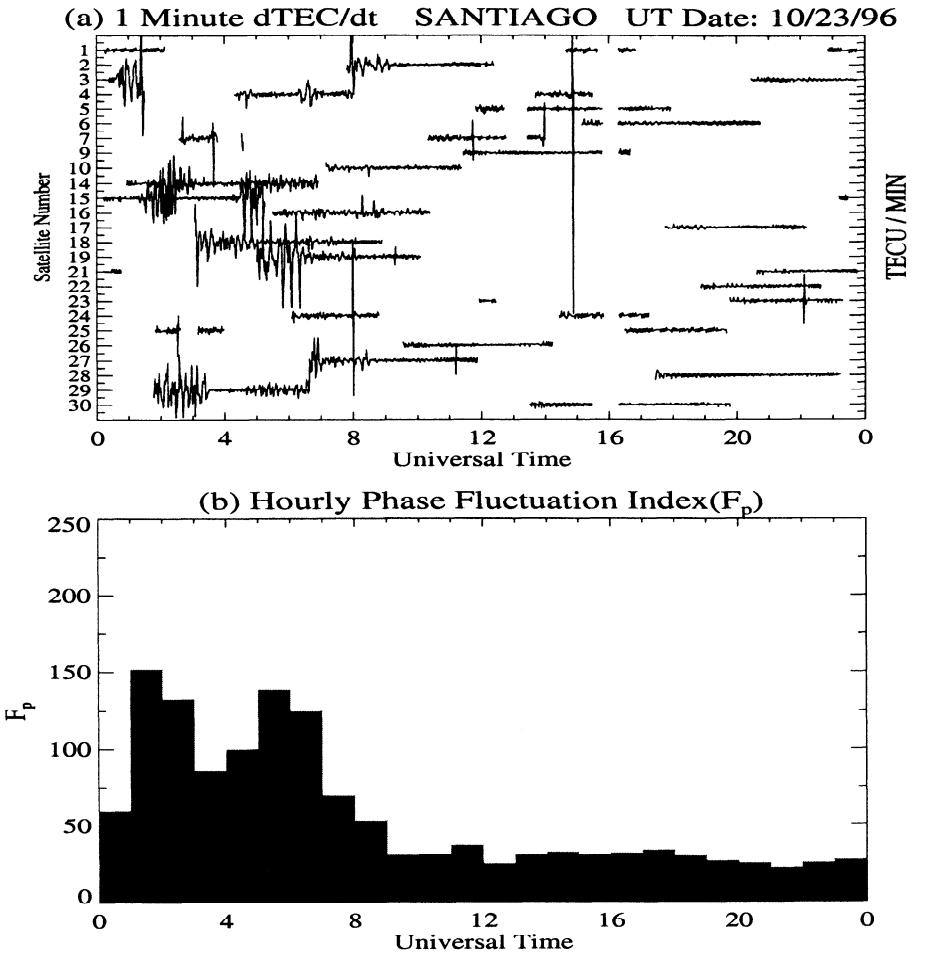

Figure 6. (a) Phase fluctuations for individual GPS satellite signals for October 23, 1996. Two periods of phase fluctuations were seen between 0100 and 0800 UT. (b) The hourly F_P index clearly captures the phase fluctuation patterns at this southern anomaly crest location and successfully suppresses noise spikes throughout the day.

3.1. Morphology of Ionospheric Equatorial Spread *F* (ESF)

It took decades of observations and analysis to uncover that ESF has an occurrence pattern based primarily on longitude and month and not on the standard paradigms for solar-terrestrial behavior: season and local time for quiet times and solar wind and magnetospheric input during disturbed times. These "ESF seasons" have been described by several authors (most recently by *Aarons* [1993] and *McClure et al.*, [1998]). Such patterns have been the basis for theoretical insights into ESF onset, defining conditions that promote or inhibit Rayleigh-Taylor instability growth rates [*Tsunoda*, 1985; *Maruyama*, 1988; *Marayama and Matuura*, 1984; *Mendillo et al.*, 1992a; *Sultan*, 1996].

As studies continue to search for the actual physical mechanisms that instigate or suppress ESF, to refine the spatial morphologies over various geomagnetic and solar cycle conditions, and to test cause-effect predictive schemes for practical applications, it would be helpful to have a readily available parameter that can capture ESF occurrence and intensity throughout the low-latitude zone at all times of the day and year. The GPS-derived F_P index defined in section 2 offers such a possibility. In so trying to

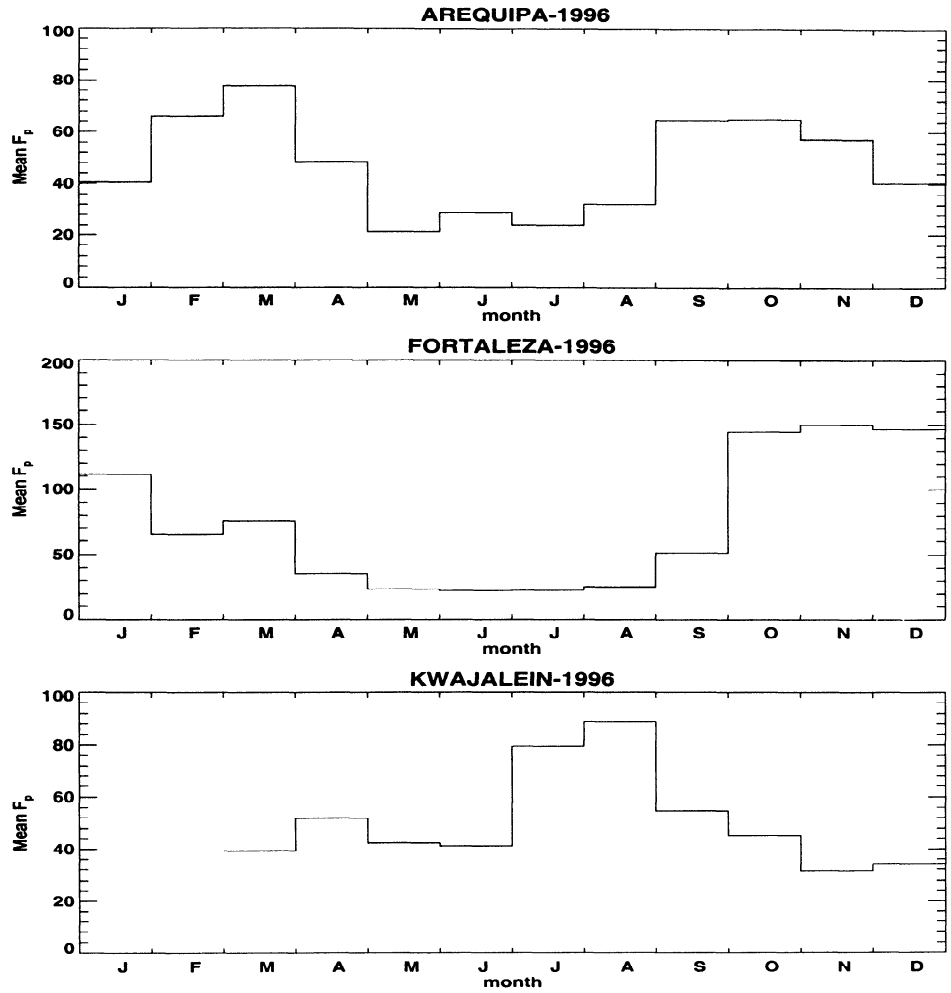

Figure 7. Monthly average $(F_P)_{\max}$ indices for Arequipa, Fortaleza, Kwajalein, 1996, showing seasonal longitude patterns. There are no data available for January and February for Kwajalein.

expand its utility, we are cautious of the pitfalls common in the use of indices in geophysics, such as the solar radio flux at 10.7 cm as a proxy for UV/EUV radiation or K_p as a description of global geomagnetic activity. As a first test, we decided to see if it captures the accepted morphology of ESF and then to determine if it adds quantitative information not previously known or appreciated.

The GPS sites at Arequipa, Peru (16°S, 71.5°W, -3.5 dip latitude), Fortaleza, Brazil (4°S, 38°W, -5.6 dip latitude), and Kwajalein, Marshall Islands (9°N, 167°E, 3.9 dip latitude), offer places where ESF morphology is well known and rather different. The Peruvian sector shows a semiannual pattern of ESF with equinoctial maxima; the Brazilian sector shows an annual pattern with a broad maxima in the months spanning December solstice, and Kwajalein has an annual pattern peaking in months near June solstice [*Aarons*, 1993]. To check on these patterns using the GPS F_P index, we first examined the solar minimum year 1996 when almost complete data sets were available at all three sites. For each day of the year the 24 hourly F_P values were examined, and the maximum value was selected. This inevitably occurred during the evening hours, most often during the dusk to midnight period, and so its association

with ESF was promising. The monthly averages of these peak daily F_P values appear in Figure 7. The results are in agreement with known patterns, as described by *Aarons* [1993], and show several other aspects as well. For example, the mean strength of F_P is nearly twice as large at Fortaleza (150 units) than at Arequipa or Kwajalein (80-90 units).

To test index portrayal patterns of ESF and geomagnetic activity, we compared a full year of daily maximum F_P values with daily Ap using the GPS site at Fortaleza where the F_P characterization of ESF was the strongest of the three longitudes sampled. The results in Figure 8 confirm that there is no simple trend between ESF and geomagnetic activity [*Sahai et al.*, 1998].

The month of October 1996 was a period of high F_P at both Arequipa and Fortaleza. Figure 9a shows the correlation of their respective daily maximum F_P values. The lack of a strong trend is consistent with ESF not being correlated on a day-by-day basis on both sides of South America [*Swartz and Woodman*, 1998]. A second month of comparison, March 1996, is shown in Figure 9b with similar results.

Finally, to portray the evolution pattern for ESF in non solar minimum years, we show in Figure 10 the Arequipa monthly average of $F_{P\max}$ results for the years 1996, 1997, and 1998, when F10.7 increased from 72 to 81 to 118. This confirms that the ESF occurrence pattern is solar cycle independent, namely, that equinox months at Peruvian longitudes show the

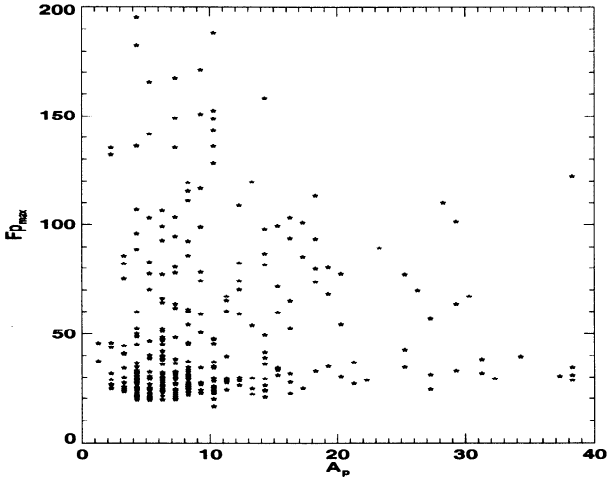

Figure 8. A comparison of daily maximum F_P values at Fortaleza, Brazil, with the geomagnetic index Ap for the year 1996.

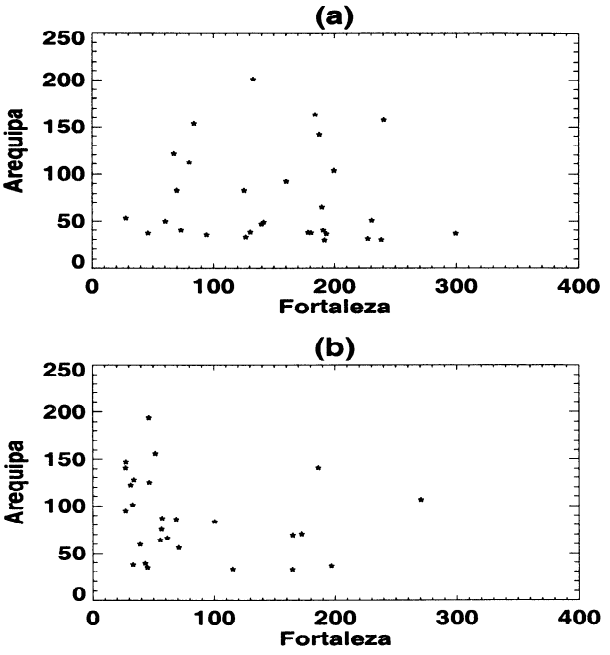

Figure 9. Comparisons of the daily maximum values of F_P at Arequipa and Fortaleza for (a) October and (b) March 1996.

most spread F; the strength of these patterns does increase with solar activity, however, and the F_P index monitors this trend in a convenient, quantitative way.

We conclude from Figures 7-10 that F_P is an index that can be used to characterize all of the known features of ESF: it portrays the seasonal longitude pattern and its solar cycle modulation; moreover, it shows the lack of correlation of ESF with geomagnetic activity and its independent occurrence rates at sites separated by 1000 km in longitude. We now proceed to use F_P in attempts to find how ESF onset might be related to precursor signatures of F region instability growth or suppression.

3.2. Prediction of ESF Using GPS TEC Morphology and Phase Fluctuation (F_P) Indices

The growth rate for the Rayleigh-Taylor instability depends on several characteristics of the low-latitude ionosphere. These include parameters describing ambient electron density gradients, collision frequencies, electrodynamical drifts, and neutral winds. In addition, a "seed perturbation" is needed to provoke the

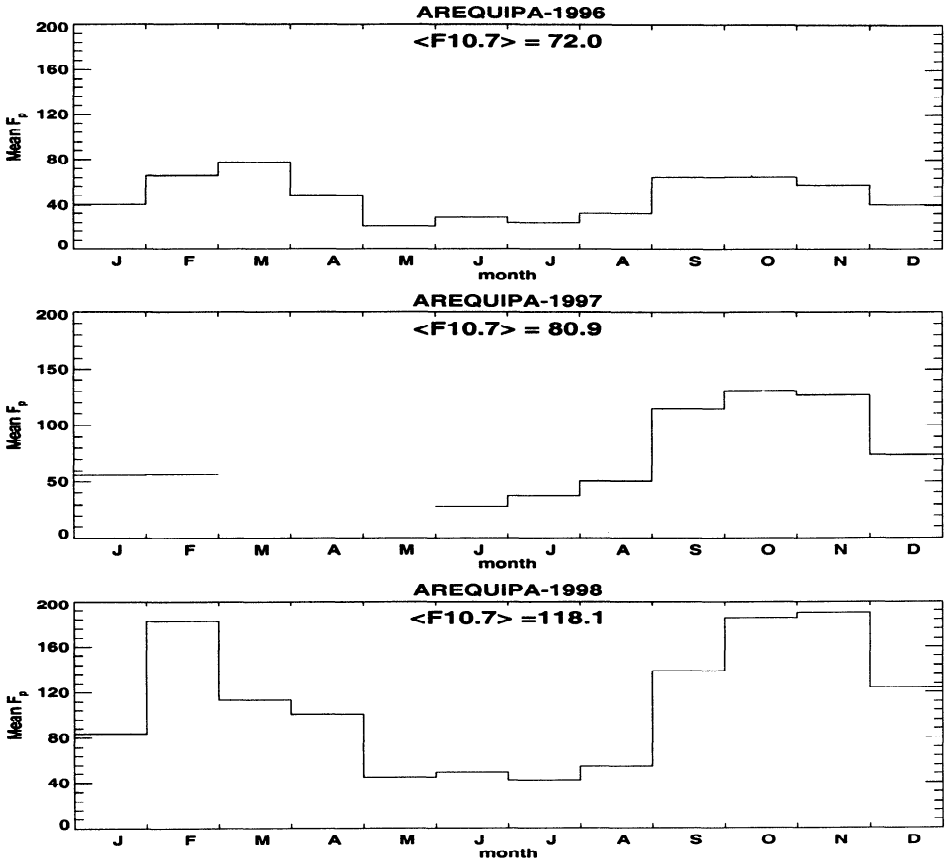

Figure 10. Monthly mean of the daily $F_{P_{\max}}$ values for Arequipa (1996-1998), showing the effects of increasing solar flux.

instability. Most simulation studies have assumed the availability of a seed perturbation and then examined the ambient plasma and dynamical conditions that would produce the fastest growth rate [*Zalesak et al.*, 1982, *Huang and Kelley*, 1996; *Kuo et al.*, 1998]. A strong vertical drift, for example, has been used in many studies to show that upward motions enhance growth rates.

Maruyama and Matuura [1984] suggested that some ambient conditions could be not just unfavorable but actually suppress ESF. In particular, they showed that a strong meridional neutral wind could do so and used seasonally dependent winds to account for the longitude monthly occurrence pattern. *Mendillo et al.* [1992a] suggested that this suppression mechanism might be pushed to day-to-day variability effects within ESF season at a given longitude and to the inhibition of ESF during magnetically active periods. *Tinsley et al.* [1997] questioned this view using a different data set from the same longitude site, and thus it is still an open issue.

The pronounced vertical drift and strong meridional wind effects upon ESF onset are mechanisms capable of being tested quantitatively. To do so, we return to Figure 5, the TEC latitude profiles of the Appleton anomaly at 1930 LT. There is sufficient day-to-day variability in the strength of the anomaly and in the asymmetry of its north versus south peak values to compare with the F_P values for each of these days. As described by *Doherty et al.* [1997], we associate the strength of the anomaly (its peak-to-trough ratio) with higher vertical drifts leading to an enhanced fountain effect. We associate N-S asymmetries with strong neutral winds moving plasma along the magnetic meridians from one hemisphere to the other. These can be quantified using two additional

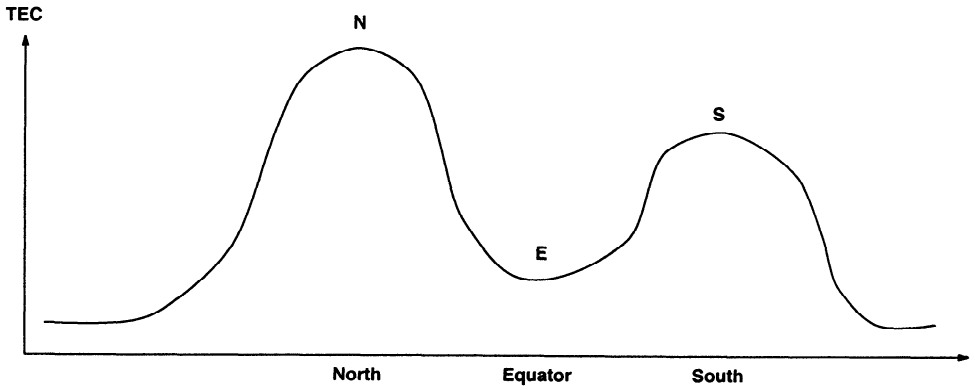

Figure 11. Schematic illustrating the derivation of a strength index I_s and an asymmetry index I_a of the Appleton anomaly in TEC.

indices, a strength index (I_s) and an asymmetry index (I_a), as defined in Figure 11. Thus, when the strength index (I_s) is large, we anticipate ESF to occur; when the asymmetry index (I_a) is large, we anticipate ESF not to occur.

We have conducted a careful data reduction of the GPS three-site chain Bogota-Arequipa-Santiago during three separate months when nearly full coverage was available at all three sites (not always the case due to equipment problems at one of the sites). The results for September 1995, October 1996 and September 1998 are given in Figure 12. Figure 12a shows comparisons of the anomaly strength index (I_s) at 1930 LT and the maximum F_P index during the subsequent 2000-2400 LT hours. There is not a strong trend in these data sets except, perhaps, in the highest solar flux year examined (1998). Using a simple characteristic of the anomaly, its TEC peak-to-trough ratio, as an indicator of strong electrodynamical vertical drift, is clearly not a reliable indicator of subsequent ESF onset. In Figure 12b, where the asymmetry index is compared to F_P, there is simply no evidence of a relationship between the two. If asymmetries in the anomaly's peak TEC values are driven by transequatorial winds, as is commonly assumed, then no evidence exists here for winds affecting ESF on a day-to-day basis. Clearly, more modeling work is needed to isolate the specific influences of electric fields and winds upon $Ne(h)$ versus latitude patterns during anomaly formation times.

Since Arequipa is a site near the geomagnetic equator, the possibility exists that F_P captures a myriad of plasma irregularity patterns that might confuse attempts to correlate it with the most dramatic form of ESF, namely, high-altitude plumes of irregularities. The GPS site at Santiago, Chile, is in the Appleton anomaly region, and thus phase fluctuations observed there pertain mainly to ESF plumes that have affected flux tubes with equatorial apex heights of 800-2000 km, well above the peak density height of the Arequipa F region [see *Aarons et al.*, 1997]. Figure 13 shows Santiago results from the same analysis and months used at Arequipa (Figure 12). Again, we see no dramatic trend in these data. There are many more days of low F_P values at Santiago, primarily because few ESF plumes reached geomagnetic field lines sampled by that site. Thus, the F_P index has a latitude dependence consistent with the physics driving the instability. The many more values of $F_P \leq 50$ also confirm that those F_P values indeed represent geophysical noise levels for ΔTEC/min. Finally, we note that the few days at Santiago of high altitude/latitude irregularities ($Fp_{\max} > 100$) exhibit a trend with the I_s and I_a indices; yet the same ranges of index values have many more days with $Fp_{\max} \leq 100$, making them of no real use as a forecasting tool.

3.3. Ionospheric Storms at Low Latitudes

Ionospheric total electron content (TEC) is a parameter well suited for studies of F region behavior during geomagnetic storms. From its earliest use

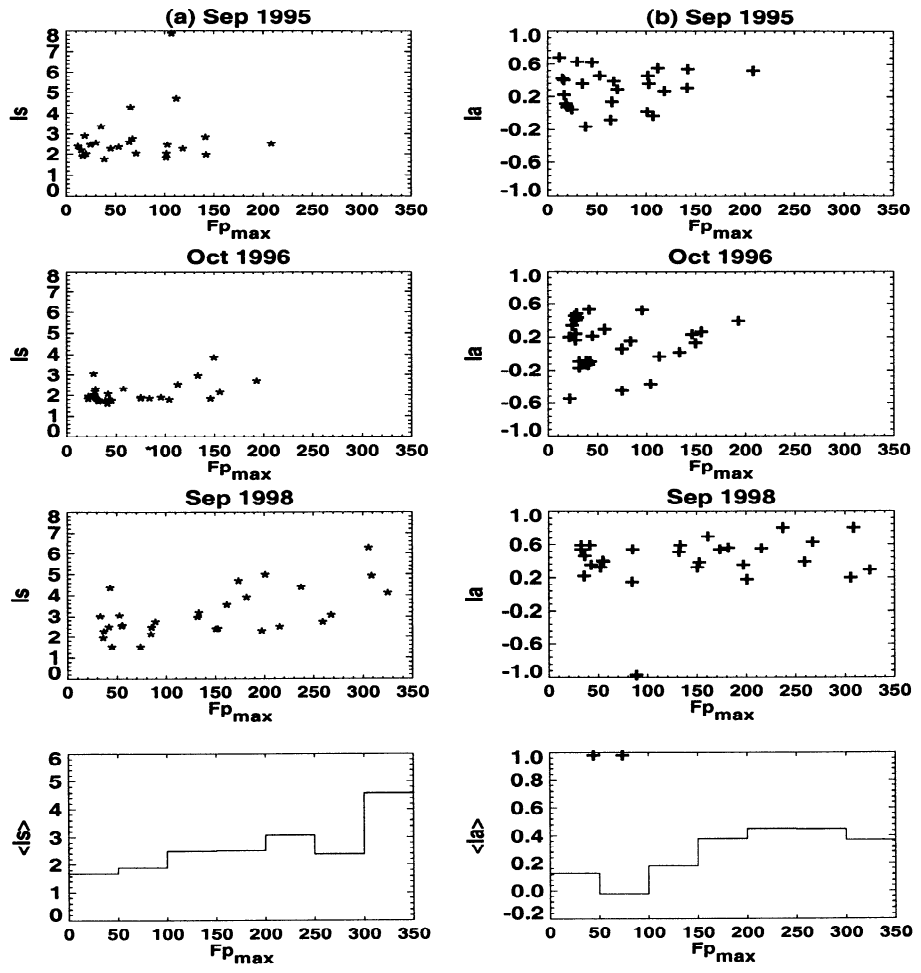

Figure 12. (a) Results of comparing the anomaly strength index I_s at 1930 LT to the maximum phase fluctuation index ($F_{P\max}$) during the subsequent 2000-2400 LT hours at Arequipa. (b) Results using the anomaly asymmetry index (I_a). Three equinox periods are shown separately and histograms of the average results over the full sample are given below.

in such studies at a single site [*Hibberd and Ross*, 1967] to its use in multisite chains of observations [*Mendillo and Klobuchar*, 1975; *Lanzerotti et al.*, 1975], past TEC studies have been the basis for significant progress in understanding the chemical and dynamical processes that cause ionospheric perturbations during geomagnetic storms (see Prolss [1995] for an excellent review of the status of ionospheric storms).

The GPS era of hundreds of sites observing TEC on a continuous, global basis offers an opportunity unprecedented in the study of ionospheric disturbances. Indeed, preliminary results of doing this have been demonstrated by *Ho et al.* [1996, 1998a, b] using global ionospheric maps (GIM) of TEC. These studies used ~60 GPS stations for the storms of November 4, 1993, and November 26, 1994, and 150 stations for the event of January 10, 1997. Results to date both confirm the global F region patterns at middle and high latitudes that were gleaned from the early analyses of ionosonde data [*Matsushita*, 1959] and extend them in the important area of latitude coupling. Most impressive is the ability of GPS-generated global ionospheric maps to capture elusive traveling atmosphere disturbance proposed by *Prolss* and *Jung* [1978] and discussed by *Prolss* [1995].

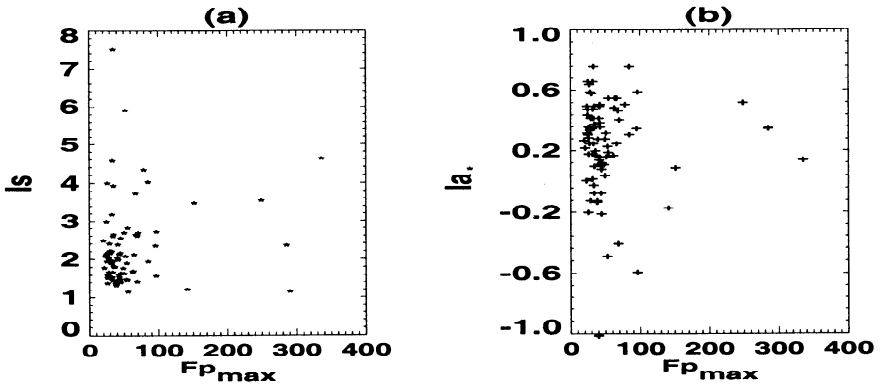

Figure 13. (a) Results of comparing the anomaly strength index I_s at 1930 LT to the maximum phase fluctuation index ($F_{P\max}$) during the subsequent 2000-2400 LT hours at Santiago. (b) Results using the anomaly asymmetry index (I_a). The periods September 1995, October 1996, and September 1998 used in Figure 12 are combined here.

Yet, as pointed out by *Ho et al.* [1998a], the major uncertainty in F region storm studies is the behavior at equatorial and low latitude where "low latitude storm effects are more difficult to distinguish from the large quiet time noise." A perusal of the monthly day-to-day variability shown for a single hour at a single site in Figure 5 confirms the problem in dramatic form.

The classic picture of an ionospheric storm is that while both positive and negative phases are found at middle and high latitudes, only positive phase effects appear at low latitudes [e.g., *Obayashi*, 1964; *Rajaram and Rostogi*, 1969]. This is due primarily to atmospheric circulation effects that create O/N_2 enhancements at low latitudes, while O/N_2 decreases account for the dominate negative phase effects at more poleward locations. Relatively simple modeling studies demonstrate the roles of chemistry and dynamics at middle latitude [*Mendillo et al.*, 1992b]. Far less attention has been paid to low latitude effects, mainly because of the lack of unambiguous morphologies to model. The equatorial zone offers, perhaps, the ultimate test case for understanding magnetosphere-ionosphere interactions due to the role of electrodynamics being so subtle and complex deep within the plasmasphere. The prompt penetration of electric fields, the creation and duration of a high-latitude shielding layer, and the delayed appearance of disturbance dynamo effects have been described by *Scherliess and Fejer* [1997, and references therein]. A consistent model for the low-latitude ionospheric storm is therefore one that cannot make simplifying assumptions about isolation from high-latitude disturbance sources.

To assess in a preliminary way the use of the GPS network in South America for storm studies, we computed diurnal curves of the six stations for periods of geomagnetically quiet ($< A_p >= 3$) and disturbed ($< A_p >= 34$) days in October 1996. These results appear in Figure 14.

While Figure 14 represents the first use of GPS data for TEC average storm studies at equatorial latitudes, by no means is it a definitive statement on storm time morphologies. It does confirm, however, that the dominant feature found in early ionosonde studies, namely, that positive phase storm effects span the full Appleton anomaly region, is captured in both individual and mean behavior of GPS-based TEC measurements.

4. Summary and Conclusions

In this paper we have shown how total electron content (TEC) data from the GPS satellites can be used to address several outstanding questions in equatorial aeronomy. Methods of observing TEC and using its behavior to study upper atmospheric processes date from the beginning of the artificial satellite era. As new radio beacon techniques became available, periods of technique testing and verification were quickly followed by applications to geophysical problems. The study of ionospheric storms,

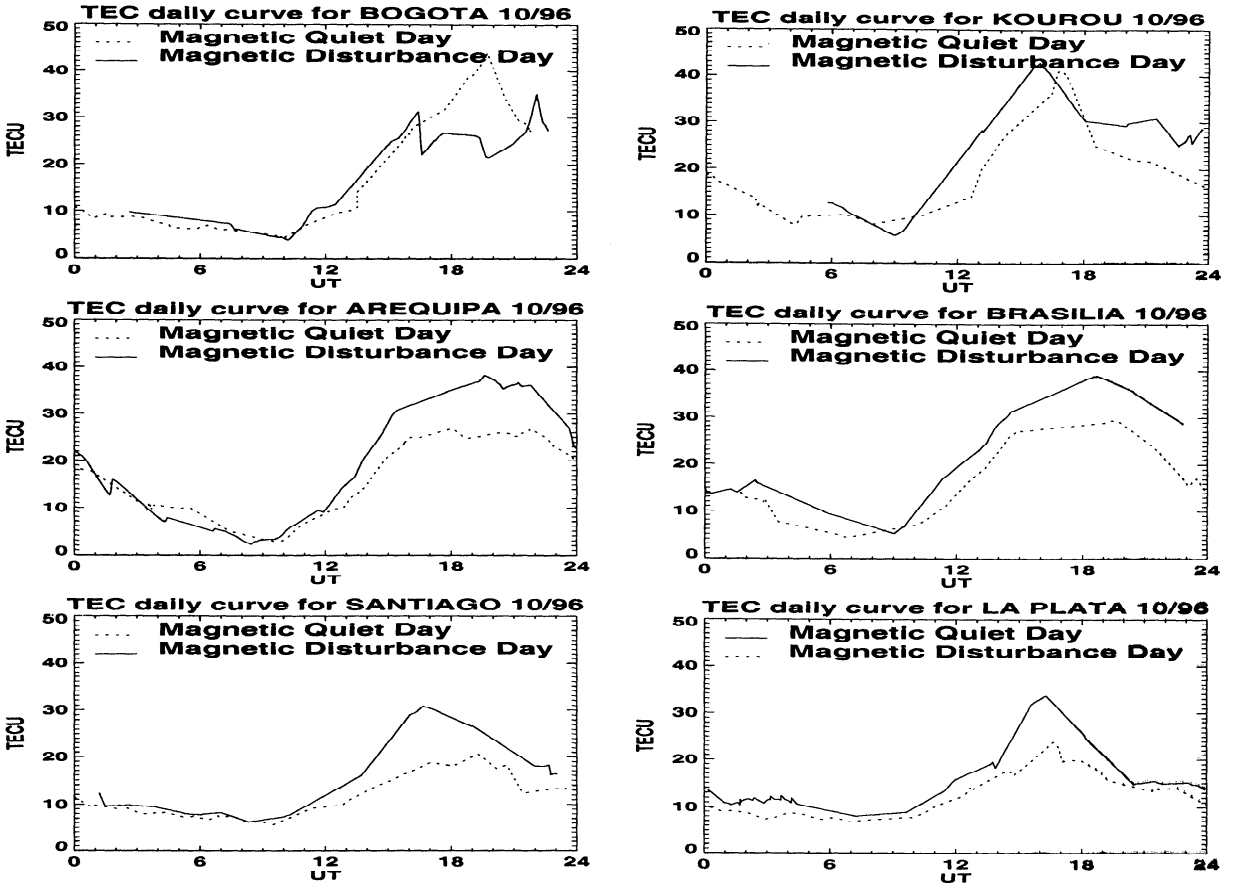

Figure 14. Comparison of average TEC daily curves for magnetically quiet days, October 5, 6, 7, and magnetically disturbance days, October 18, 22, 23, 1996, with mean *Ap* values of 3 and 34, respectively.

in particular, came early in the study of TEC behavior, starting with the study of *Hibberd and Ross* [1967]. With the GPS methods now clearly beyond its technique verification phase, the field is poised to address physical processes, as done in the recent study of *Lu et al.* [1998].

In the present work, where a network of low latitude stations spanning South America was used, it was shown that the "classic" pattern of enhanced TEC occurs in a very limited statistical study of a few days of geomagnetic activity. The key to understanding ionospheric storms at low latitudes is probably in understanding the severe events, when typical seasonal and local time dependent storm onset effects, well known at midlatitudes, extend into the low-latitude domain. That the equatorial region is dominated by the Appleton anomaly should not be forgotten in conducting storm studies, for storm-induced electrodynamics may be as effective a source of perturbations as neutral composition changes are, as pointed out 30 years ago by *Rajaram and Rastogi* [1969].

A unique use of GPS data has been the study of phase fluctuations associated with 30 s changes in TEC. At low latitudes this is a significant addition to the traditional ways of monitoring F region plasma irregularities via amplitude scintillation or radar backscatter associated with classical equatorial spread F (ESF) disturbances. Building upon previous attempts to define useful descriptions of TEC fluctuation, we developed new 15 min and hourly phase fluctuation indices that capture both the spa-

tially confined and stationwide/all-sky patterns in quantitative ways. These have been used to demonstrate successful "now casting" methods for the specification of irregularities and for the quantitative, statistical description of ESF occurrence patterns versus longitude, season, and solar cycle. An attempt was made to use the GPS-derived equatorial ionization anomaly morphology of TEC as an indicator of the thermospheric winds and electrodynamical drifts that affect ESF occurrence. The forecast of ESF using such indicators at dusk were not particularly successful, as verified by subsequent GPS phase fluctuations in the premidnight hours. The day-to-day variation of ESF remains elusive, and more modeling of wind and electric field effects upon the tropical F region are needed to guide the potential use of integrated plasma contents in the forecast of instability patterns.

An area of study not addressed here is the relationship between ESF and geomagnetic activity during the postmidnight hours. It is generally accepted that this is the only LT period when the two are correlated, namely, that ESF onset effects occur when magnetic activity is high [*Rastogi and Woodman*, 1978]. A comprehensive understanding of this relationship will surely contribute to our attempts to link ESF onset to F region morphology in the dusk-to-midnight sector.

Acknowledgments. This work was supported in part by grants from NASA, the Office of Naval Research, and the National Science Foundation. We are grateful to Xiaoqing Pi at JPL for discussions and assistance on access and use of online GPS data. Patricia Doherty of Boston College offered advice and assistance in the analysis of GPS data and Santimay Basu valuable scientific discussions. In particular, we acknowledge the years of effort and collegial assistance of John Klobuchar in fostering use of GPS data for scientific analysis.

References

Aarons, J., The longitudinal morphology of equatorial F layer irregularities relevant to their occurrence, *Space Sci. Rev., 63,* 209-243, 1993.

Aarons, J., Global positioning system phase fluctuations at auroral latitudes, *J. Geophys. Res., 102,* 17,219-17,231,1997.

Aarons, J., M. Mendillo, and R. Yantosca, GPS phase fluctuations in the equatorial region during the MISETA 1994 campaign *J. Geophys. Res., 101,* 26,851-26,862, 1996.

Aarons, J., M. Mendillo, and R. Yantosca, GPS phase fluctuations in the equatorial region during sunspot minimum, *Radio Sci., 32,* 1535-1550, 1997.

Almeida, O. G., Protonospheric columnar electron content determination, 2, Observations, *J. Atmos. Terr. Phys., 36,* 305, 1974.

Anderson, D., A theoretical study of the ionospheric F region equatorial anomaly, II, Results in the American and Asian sectors, *Planet. Space Sci., 21,* 421-442, 1973.

Anderson, D., Modeling ambient low-latitude F region ionosphere: A review, *J. Atmos. Terr. Phys., 43,* 753-762, 1981.

Anderson, D., et al., Intercomparison of physical models and observations of the ionosphere, *J. Geophys. Res., 103,* 2179-2192, 1998.

Basu, S., Su. Basu, J. Aarons, J. P. McClure, and M. D. Cousins, On the coexistence of kilometer- and meter-scale irregularities in the nighttime equatorial F region, *J. Geophys. Res., 83,* 4219-4226, 1978.

Beach, T. L., and P. M. Kintner, Simultaneous global positioning system observations of equatorial scintillations and total electron content fluctuations, *J. Geophys. Res., 104,* 22,553-22,565, 1999.

Ciraolo, L., and P. Spalla, Comparison of ionospheric total electron content from the Navy Navigation Satellite System and the GPS, *Radio Sci., 32,* 1071-1080, 1997.

Coker, C., R. Hunsucker, and G. Lott, Detection of auroral activity using GPS satellites, *Geophys. Res. Lett., 22,* 3259-3262, 1995.

Davies, K., Recent progress in satellite radio beacon studies with particular emphasis on the ATS-6 radio beacon experiment, *Space Sci. Rev., 25,* 357-430, 1980.

Doherty, H. P., D. Anderson, and J. Klobuchar, Total electron content over the Pan-American longitudes: March-April 1994, *Radio Sci., 32,* 1597-1605, 1997.

Hibberd, F. H., and W. J. Ross, Variations in total electron content and other ionospheric parameters associated with magnetic storms, *J. Geophys. Res., 72,* 5331-5337, 1967.

Ho, C. M., A. J. Mannucci, U. J. Lindqwister, X. Pi and B. Tsurutani, Global ionospheric perturba-

tions monitored by the worldwide GPS network, *Geophys. Res. Lett., 23,* 3219-3222, 1996.

Ho, C. M., B. D. Wilson, A. J. Mannucci, U. J. Lindqwister, and D. N. Yuan, A comparative study of ionospheric total electron content measurements using global ionospheric maps of GPS, TOPEX radar, and the Bent model, *Radio Sci., 32,* 1499-1512, 1997.

Ho, C. M., A. J. Mannucci, U. J. Lindqwister, X. Pi, B. T. Tsurutani, L. Sparks, B. A. Iijima, B. D. Wilson, I Harris, and M. J. Reyes, Global ionospheric TEC variations during January 10, 1997 storm, *Geophys. Res. Lett., 25,* 2589-2592, 1998a.

Ho, C. M., A. J. Mannucci, L. Sparks, X. Pi, U. J. Lindqwister, B. D. Wilson, B. A. Iijima, and R. J. Reyes, Ionospheric total electron content perturbations monitored by the GPS global network during two northern hemisphere winter storms, *J. Geophys. Res., 103,* 26,409-26,420, 1998b.

Huang, C.-S., and M. C. Kelley, Nonlinear evolution of equatorial spread *F*, 2, Gravity wave seeding of Rayleigh-Taylor instability, *J. Geophys. Res., 101,* 293-302, 1996.

Imel, D. A., Evaluation of TOPEX/Poseidon dual-frequency ionosphere correction, *J. Geophys. Res.,* 99, 24,895-24,906, 1994.

Kelley, M. C., *The Earth's Ionosphere,* Academic, San Diego, Calif., 1989.

Kersley, L., and J. A. Klobuchar, Comparison of protonospheric electron content measurements from the American and European sectors, *Geophys. Res. Lett., 5,* 123-126, 1978.

Kuo, F. S., S. Y. Chou, and S. J. Shau, Comparison of topside and bottomside irregularities in equatorial *F* region ionosphere, *J. Geophys. Res., 103,* 2193-2199, 1998.

Lanyi, G., and T. Roth, A comparison of mapped and measured total ionospheric electron content using global positioning system and beacon satellite observations, *Radio Sci., 23,* 483-492, 1988.

Lanzerotti, L. J., L. L. Cogger, and M. Mendillo, Latitude dependence of ionosphere total electron content: Observations during sudden commencement storms, *J. Geophys. Res., 80,* 1287-1306, 1975.

Lu, G., S. Pi, A. D. Richmond, and R. G. Roble, Variations of total electron content during geomagnetic disturbances: A model/observation comparison, *Geophys. Res. Lett., 25,* 253-256, 1998.

Mannucci, A. J., B. D. Wilson, D. N. Yuan, C. M. Ho, U. J. Lindqwister, and T. F. Runge, A global mapping technique for GPS-derived ionospheric total electron content measurements, *Radio Sci., 33,* 565-582, 1998.

Maruyama, T., A diagnostic model for equatorial spread *F*, 1, Model description and application to electric field and neutral wind effects, *J. Geophys. Res., 93,* 14,611-14,622, 1988.

Maruyama, T., and N. Matuura, Longitudinal variability of annual changes in activity of equatorial spread *F* and plasma bubbles, *J. Geophys. Res., 89,* 10,903-10,912, 1984.

Matsushita, S., A study of the morphology of ionospheric storms, *J. Geophys. Res., 64,* 305-322, 1959.

McClure, J. P., S. Singh, D. K. Bamgboye, F. S. Johnson, and H. Kil, Occurrence of equatorial *F* region irregularities: Evidence for tropospheric seeding, *J. Geophys. Res., 103,* 29,119-29,135, 1998.

Mendillo, M. and J. A. Klobuchar, An atlas of the mid-latitude *F* region response to geomagnetic storms, *Tech. Rep., 74-0065,* Air Force Cambridge Res. Lab., Bedford, Mass., Feb. 1974.

Mendillo, M., J. A. Klobuchar, and H. Hajeb-Hosseinieh, Ionospheric disturbances: Evidence for the contraction of the plasmapause during severe geomagnetic storms, *Planet. Space Sci., 22,* 223-236, 1974.

Mendillo, M., and J. A. Klobuchar, Investigations of the ionospheric *F* region using multistation total electron content observations, *J. Geophys. Res., 80,* 643-650, 1975.

Mendillo, M., and J. Baumgardner, X. Pi, and P. J. Sultan, Onset conditions for equatorial spread *F*, *J. Geophys. Res., 97,* 13,865-13,876, 1992a.

Mendillo, M., X. He, and H. Rishbeth, How the effects of winds and electric fields in F2-layer storms vary with latitude and longitude, *Planet. Space Sci., 40,* 595-606, 1992b.

Obayashi, T., *Research in Geophysics,* edited by H. Odishaw, chap. 14, MIT Press, Cambridge, Mass., 1964.

Pi, X., A. J. Mannucci, U. J. Lindqwister, and C. M. Ho, Monitoring of global ionospheric irregularities using the worldwide GPS network, *Geophys. Res. Lett., 24,* 2283-2286, 1997.

Prolss, G. W., Ionospheric *F* region storms, in *Handbook of Atmospheric Electrodynamics,* vol. 2, edited by H. Volland, 195-248, CRC Press, Boca Raton, Fla., 1995.

Prolss, G. W., and M. J. Jung, Traveling atmospheric disturbances as a possible explanation for daytime positive storm effects of moderate duration at middle latitudes, *J. Atmos. Terr. Phys., 40,* 1351-1354, 1978.

Rajaram, G., and R. G. Rastogi, A synoptic study of the distributed ionosphere during IGY-IGC-(1) the Asian Zone, *Ann. Geophys., 25,* 795-805, 1969.

Rastogi, R. G., and R. F. Woodman, Spread *F* in equatorial ionograms associated with reversal of horizontal *F* region electron field, *Ann. Geophys., 34,* 31-36, 1978.

Sahai, Y., P. R. Fagundes, J. A. Bittencourt, and M. A. Abdu, Occurrence of large scale equatorial *F* region plasma depletions during geomagnetic disturbances, *J. Atmos. Terr. Phys., 60,* 1593-1604, 1998.

Scherliess, L., and B. Fejer, Storm time dependence of equatorial disturbance dynamo zonal electric fields, *J. Geophys. Res., 102,* 24,037-24,046, 1997.

Sultan, P. J., Linear theory and modeling of the Rayleigh-Taylor instability leading to the occurrence of equatorial spread *F*, *J. Geophys. Res., 101,* 26,875-26,891, 1996.

Swartz, W. E., and R. F. Woodman, Same night observations of spread *F* by the Jicamarca Radio Observatory in Peru and CUPRI in Alcantara, Brazil, *Geophys. Res. Lett., 25,* 17-20, 1998.

Tinsley, B. A., R. P. Rohrbaugh, W. B. Hanson, and A. L. Broadfoot, Images of transequatorial *F* region bubbles in 630- and 777-nm emissions compared with satellite measurements, *J. Geophys. Res., 102,* 2057-2077, 1997.

Titheridge, J. E., Determination of ionospheric electron content from the Faraday rotation of geostationary satellite signals, *Planet. Space Sci., 20,* 353-369, 1972.

Tsunoda, R. T., Control of the seasonal and longitudinal occurrence of equatorial scintillations by the longitudinal gradient in integrated *E* region Pedersen conductivity, *J. Geophys. Res., 90,* 447-456, 1985.

Wanninger, L., Ionospheric monitoring using IGS data, paper presented at the IGS Workshop, Inst. of Geol. Sci., Bern, Switzerland, March 1993.

Wilson, B. D., A. J. Mannucci, and C. D. Edwards, Subdaily northern hemisphere maps using an extensive network of GPS receivers, *Radio Sci., 30,* 639-648, 1995.

Yeh, K. C., and C. H. Liu, Radio wave scintillation in the ionosphere, *Proc. IEEE, 70,* 324, 1982.

Zalesak, S. T., S. L. Ossakow, and P. K. Chaturvedi, Nonlinear equatorial spread *F*: The effect of neutral winds and background Pedersen conductivity, *J. Geophys. Res., 87,* 151-166, 1982.

J. Aarons, B. Lin, and M. Mendillo, Center for Space Physics, Boston University, Room 506, 725 Commonwealth Avenue, Boston MA, 02215. (aarons@buasta.bu.edu; lbs@bu.edu)

(Received May 18, 1999; revised December 21, 1999; accepted January 3, 2000.)